Volume 7
Number 8
21 April 2025
Pages 2121–2384

Nanoscale Advances

rsc.li/nanoscale-advances

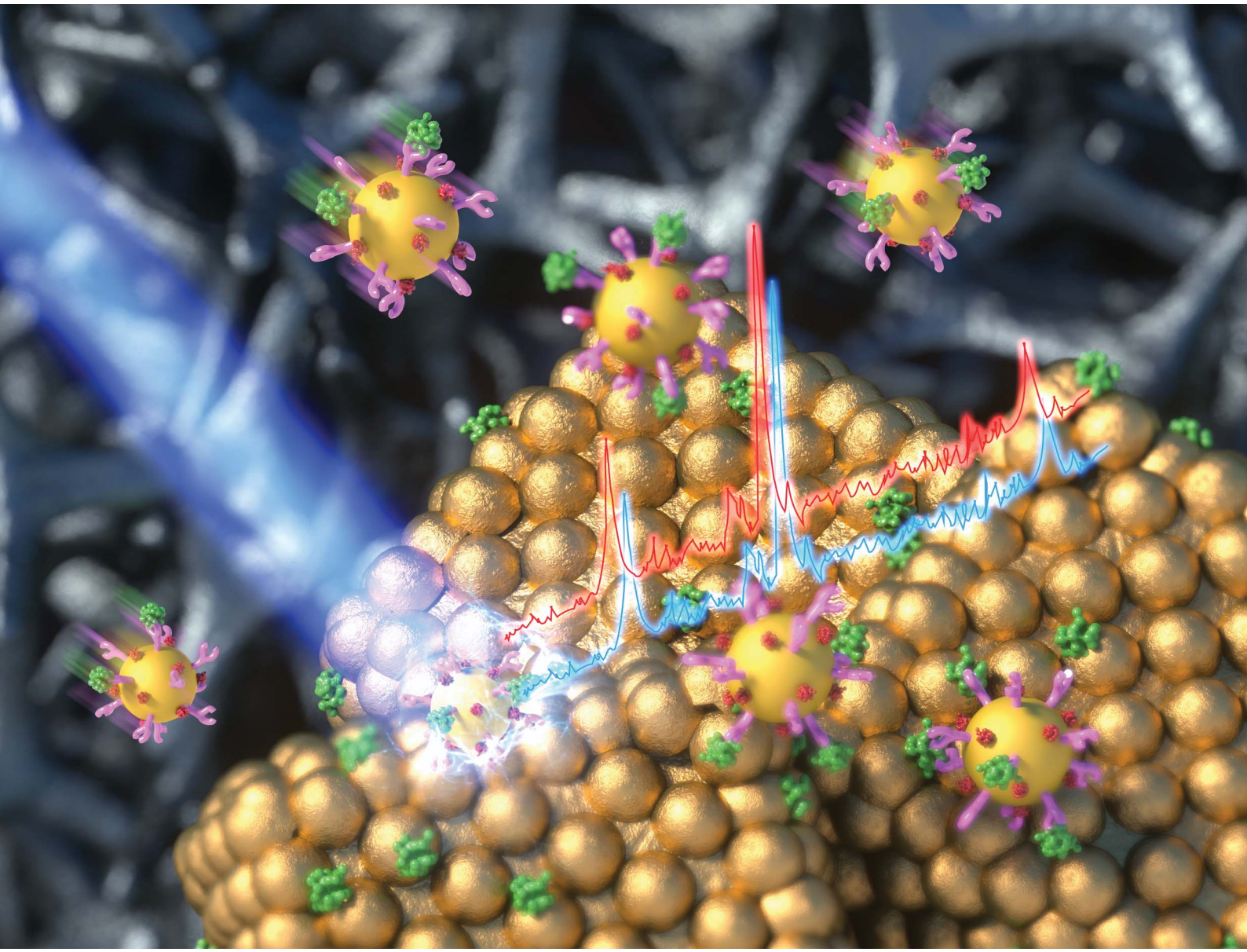

ISSN 2516-0230

ROYAL SOCIETY OF CHEMISTRY

PAPER

Seunghyun Lee *et al.*

Highly sensitive SERS-active substrate with uniform gold nanostructures on heat-treated Ni foam for detection of cardiovascular disease biomarker

NCNST

Nanoscale Advances

ROYAL SOCIETY OF CHEMISTRY

PAPER

View Article Online
View Journal | View Issue

Open Access Article. Published on 13 March 2025. Downloaded on 1/10/2026 1:36:28 PM.
This article is licensed under a Creative Commons Attribution-NonCommercial 3.0 Unported Licence.

Check for updates

Cite this: *Nanoscale Adv.*, 2025, **7**, 2171

Highly sensitive SERS-active substrate with uniform gold nanostructures on heat-treated Ni foam for detection of cardiovascular disease biomarker†

Sunghoon Yoo,‡[ac] Jaejun Park,‡[ac] Dong Hwan Nam,[ac] Sumin Kim,[ac] Dongtak Jeong,[d] Moon-Keun Lee[e] and Seunghyun Lee *[abc]

Received 14th January 2025
Accepted 22nd February 2025

DOI: 10.1039/d5na00052a

rsc.li/nanoscale-advances

Surface-enhanced Raman scattering (SERS) immunoassays for biomarker detection have attracted considerable attention owing to their high sensitivity and selectivity. In this study, we fabricated hotspot-rich SERS-active substrates by depositing gold after forming a protruding structure on the surface *via* high-temperature heat treatment. The structure formed by the heat treatment enabled a more uniform and dense gold nanostructure, which provided more hotspots within the focal volume of the Raman laser, thereby enhancing the SERS signal. This was verified by calculating the electromagnetic field using a finite element method. The fabricated SERS-active substrates and 50 nm gold nanoparticles were used to perform a competitive assay for the detection of cardiac troponin I (cTnI). The assay demonstrated a cTnI detection range of 10^0–10^6 pg mL^{-1} with a detection limit of 5.8 pg mL^{-1}. This indicates that the SERS-active substrate fabricated from the Ni foam has the potential to be used as a sensitive and selective tool for the detection of various biomarkers in complex biological samples.

Introduction

Acute myocardial infarction (AMI) is a serious cardiovascular disease that requires rapid and accurate diagnosis. Cardiac troponin I (cTnI) has been identified as a more specific and sensitive biomarker for diagnosing acute MI than other biomarkers. cTnI reaches detectable concentrations within 3 to 6 h after AMI and remains in the bloodstream for up to 10 days, necessitating the use of rapid and sensitive detection technology.[1–3]

Nanotechnology-based biosensors employing various methodologies, including electrochemistry,[4–9] fluorescence,[10–15] and enzyme-linked immunosorbent assay (ELISA),[16–20] are currently being investigated for the purpose of detecting biomarkers, including cTnI. Electrochemical methods exhibit high detection sensitivity but are susceptible to instability, inefficiency, and electrode passivation. Fluorescence assays demonstrate high specificity but are limited by low detection accuracy and poor sensitivity to photobleaching. ELISA, on the other hand, offers the advantages of simplicity and rapidity, but it is dependent on enzyme activity and lacks sensitivity. Although the aforementioned assays have been extensively utilized to detect cTnI, these shortcomings have prompted considerable interest in surface-enhanced Raman scattering (SERS) technology, an alternative nanotechnology-based biosensor that can compensate for these shortcomings.

SERS is a highly sensitive molecular detection technique that enhances Raman scattering of molecules adsorbed on metal surfaces or nanostructures.[21–30] Simply put, SERS is a surface analysis technique that overcomes the disadvantages of conventional weak Raman signals by using signals amplified by plasmonic nanoparticles or nanostructures to detect small amounts of analytes quickly and with high sensitivity. SERS has several advantages over conventional analytical techniques. First, it is non-destructive, allowing repeated analyses without damaging the sample; second, the analysis time is short; third, it can identify and analyze biomarkers based on the fingerprint information inherent in biomolecules; fourth, it has a high specificity at the molecular level; and fifth, it has high analytical accuracy owing to a much narrower peak bandwidth. These advantages make SERS an excellent sensor to replace the aforementioned analytical methods. Many studies have used SERS to detect cTnI. The Khlebtsov *et al.* developed a SERS-based lateral flow immunoassay using gold nanorod cores with GERTs between the gold shell, achieving a detection limit

[a]*Department of Applied Chemistry, Hanyang University ERICA, Ansan, 15588, Republic of Korea. E-mail: leeshyun@hanyang.ac.kr*

[b]*Department of Chemical and Molecular Engineering, Hanyang University ERICA, Ansan, 15588, Republic of Korea*

[c]*Center for Bionano Intelligence Education and Research, Hanyang University ERICA, Ansan, 15588, Republic of Korea*

[d]*Department of Medicinal & Life Science, College of Science and Convergence Technology, Hanyang University ERICA, Ansan, 15588, Republic of Korea*

[e]*Center for Nano Bio Development, National NanoFab Center, Daejeon, 34141, Republic of Korea*

† Electronic supplementary information (ESI) available. See DOI: https://doi.org/10.1039/d5na00052a

‡ These authors contributed equally.

© 2025 The Author(s). Published by the Royal Society of Chemistry

Open Access Article. Published on 13 March 2025. Downloaded on 1/10/2026 1:36:28 PM.
This article is licensed under a Creative Commons Attribution-NonCommercial 3.0 Unported Licence.

of 0.1 ng mL^{-1}.[31] The Cheng *et al.* reported a detection limit of 8.9 pg mL^{-1} using Au@Ag core–shell nanoparticles and gold patterned chips.[1] Additionally, the Bai group demonstrated a detection limit of 0.09 ng mL^{-1} using Au@Ag–Au nanoparticles as nanoprobes in their SERS-based lateral flow analysis.[32] Consequently, SERS-based immunoassays have been extensively employed to identify a plethora of biomarkers in analytical research, clinical diagnostics, and environmental monitoring, including DNA, RNA, peptides, and proteins.

To achieve the greatest SERS effect, it is necessary to create a significant number of hotspots, which are highly localized regions with intense local field enhancement. This phenomenon is thought to be caused by local surface plasmon resonances.[33–36] The formation of hotspots is contingent on the strength of the plasmonic coupling between metal nanoparticles or nanostructures. The size, shape, spacing, and distribution of metal structures influence the formation of hotspots. The key to amplifying the Raman signal in SERS is to control these factors to create uniform hotspots on a large surface area. Therefore, to achieve the greatest amplification of surface plasmon intensity, it is of paramount importance to select and place appropriate structures that can form hotspots. Various research groups have reported the development of highly sensitive SERS substrates. The Lee group successfully detected benzene thiol at 10^{-9} M by creating ring-shaped hot lines between the substrate and gold nanoparticles using a V-shaped anodic aluminum oxide (AAO) template.[23] The Tan group achieved detection of rhodamine 6G at 1 μM concentration by systematically arranging nanostructure arrays and optimizing the spacing between nanostructures using CMOS-compatible silicon technology.[37] Additionally, the Lee group demonstrated the possibility of detecting 4-mercaptophenol at 10 fM levels by introducing gold nanoparticles to vertically aligned carbon nanotubes.[38] These previous studies showed good SERS efficiency by controlling the spacing of the hotspots.

A nickel (Ni) foam template with a high specific surface area and porous structure was employed to fabricate the SERS-active substrates. A protruding grain structure was formed on the surface of the Ni foam by high-temperature heat treatment, and gold was then deposited to form hemispherical structures with a diameter of 20 nm and a high density on the grain structure. The grain structure formed by heat treatment has a lower surface energy, which allows gold to be uniformly deposited, resulting in high reproducibility of the signal. When measuring Raman spectra, it is advantageous to maximize the number of uniform hotspots in the focal volume of the Raman laser. Therefore, the formation of hotspots on the grain structure by heat treatment is a significant advantage for SERS signal enhancement. In other words, SERS substrates with a protruding grain structure formed by heat treatment exhibited a higher level of Raman signal enhancement than those without heat treatment. The experimental and theoretical results indicate that SERS-active substrates with a grain structure formed by heat treatment followed by gold deposition are highly sensitive and reproducible.

In this study, we used a Ni foam-based three-dimensional SERS-active substrate with uniform and dense hotspots to detect cardiac biomarkers for heart failure prognosis. A competitive assay was used to detect cTnI by employing a monoclonal antibody to detect cTnI. While sandwich assays employing polyclonal antibodies can provide relatively high sensitivity, competitive assays utilizing monoclonal antibodies have the advantages of high specificity and selectivity, as they react solely with a single site (epitope) on the target molecule.[39] In this experiment, the competitive assay confirmed a linear relationship between cTnI concentration and SERS intensity, and a limit of detection (LOD) of 5.8 pg mL^{-1} was obtained.

Results and discussion

We fabricated SERS-active substrates with high density and uniform hotspots using Ni foam with a high specific surface area and porous structure as a template. The fabrication process involved the formation of protruding grains on the surface *via* high-temperature heat treatment, followed by the deposition of gold. Fig. 1 schematically depicts this process, showing the formation of the SERS-active substrate. Prior to the use of the Ni foam in this process, the surface was cleaned with HCl to remove impurities. This process is known to improve the surface roughness of Ni foam and strengthen the adhesion

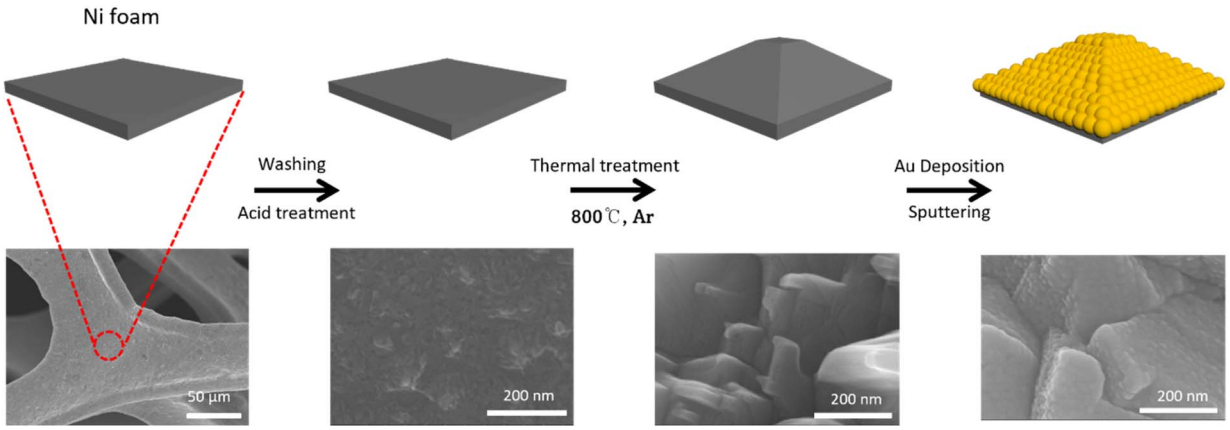

Fig. 1 Schematic showing the development of the SERS-active substrate based on Ni foam.

 © 2025 The Author(s). Published by the Royal Society of Chemistry

Open Access Article. Published on 13 March 2025. Downloaded on 1/10/2026 1:36:28 PM.
This article is licensed under a Creative Commons Attribution-NonCommercial 3.0 Unported Licence.

between Ni foam and gold during gold deposition.[40] Subsequent heat treatment at 800 °C using TCVD changes the surface roughness of the Ni foam, resulting in the formation of a protruded grain structure.[41] Because oxygen exposure during the heat-treatment process caused a nickel oxide layer to form on the surface of the Ni foam, Ar gas was used to prevent the formation of the oxide layer. The surface morphology of the Ni foam transformed over time during heat treatment. After 30 min of heat treatment at 800 °C, a small grain structure (≈100 nm) was formed on the surface of the Ni foam. However, after 7 h, a large grain structure (≈400 nm) formed. With increasing heat-treatment time, the change in the surface morphology became more pronounced as the surface of the Ni foam melted. Gold was deposited on the Ni foam by sputtering for 600 s at 20 mA with a thickness of 0.6 Å s^{-1}, forming varying grain structures depending on the heat-treatment time.

Fig. 2a and b show SEM images of the grain structure formed on the Ni foam surface as a function of heat-treatment time (Fig. $2a_1$–a_5) and SEM images of gold deposited on the surface for 600 s after heat treatment (Fig. $2b_1$–b_5). The shape of the deposited gold depends on the size of the grain structure formed during heat treatment. The size of the protruding grain structure varied with heat treatment time, which changed the geometry of the deposited gold. In the large-grain structure formed after 7 h of heat treatment, Au was uniformly deposited in the form of hemispheres. By contrast, in the small-grain structure formed after 30 min of heat treatment, gold was deposited unevenly owing to the agglomeration of atoms during

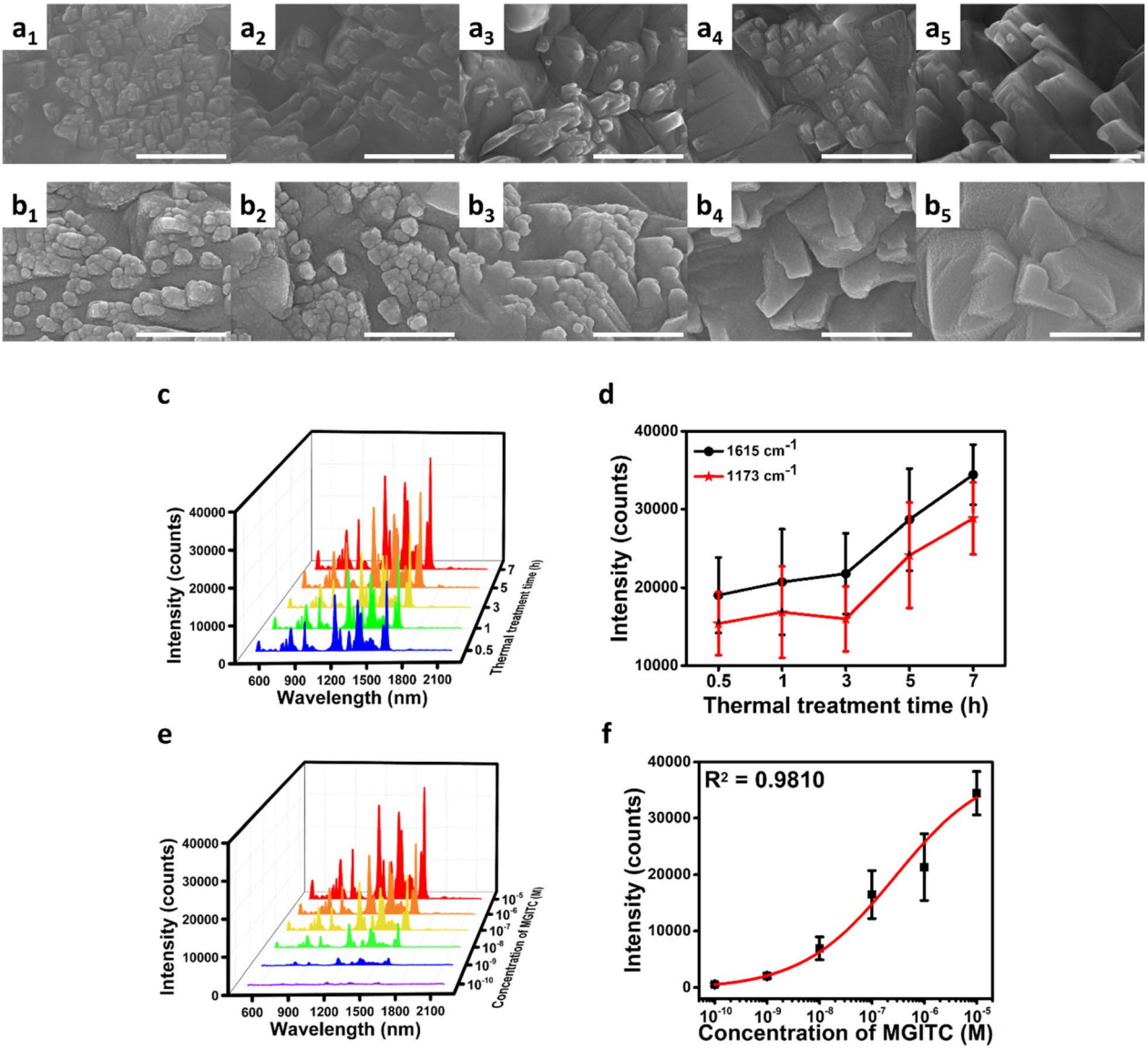

Fig. 2 (a_1–a_5) SEM images of the protruding structure formed on the Ni foam surface according to heat-treatment time (0.5, 1, 3, 5, and 7 h, respectively). (b_1–b_5) SEM images of the gold deposited after heat treatment. The scale bar represents 500 nm. (c) Comparison of SERS signals observed in (b_1–b_5). (d) Corresponding calibration curves for the SERS peak intensities at 1173 and 1615 cm^{-1}, the signature peaks of MGITC. (e) Average SERS spectrum observed in (b_5); (f) corresponding calibration curve for varying concentrations of MGITC.

Open Access Article. Published on 13 March 2025. Downloaded on 1/10/2026 1:36:28 PM.
This article is licensed under a Creative Commons Attribution-NonCommercial 3.0 Unported Licence.

deposition. This is because the longer the heat-treatment time, the lower the surface energy, which results in a more uniform and dense deposition of gold atoms. SEM image and EDS spectra of the substrate with gold deposited on the grain structure formed after 7 hours of heat treatment are shown in Fig. S1.† To establish the conditions for fabricating optimal SERS-active substrates, we deposited gold on Ni foam after 0.5–7 h of heat treatment and compared the SERS signals using MGITC as a Raman probe molecule. Fig. 2c shows that the SERS signal intensity increased as the heat treatment time increased from 0.5 to 7 h. To facilitate comparison, the intensity changes in the SERS spectra at 1173 and 1615 cm^{-1}, the characteristic Raman peaks of MGITC, were evaluated (Fig. 2d). At 1173 cm^{-1}, the number of counts increased from 15 391 at 0.5 h to 28 847 at 7 h, representing an ≈1.87-fold increase. At 1615 cm^{-1}, the number of counts increased from 19 033 at 0.5 h to 34 439 at 7 h, representing an ≈1.80-fold increase. In other words, the intensities of the two main peaks of MGITC (1173, 1615 cm^{-1}) increased with the increase in heat-treatment time, thereby confirming that the gold-deposited substrate after 7 h of heat treatment had a higher SERS efficiency. Fig. 2e and f illustrate the variation in SERS signal with MGITC concentration, confirming that the SERS efficiency was optimal when gold was deposited after 7 h of heat treatment. A comparison of the SERS signal as a function of the MGITC concentration revealed the presence of a considerably low concentration of MGITC (≈100 pM). Furthermore, a reasonable trend in the signal was observed, with an R^2 value of 0.988 for the concentration-dependent calibration curve at 1615 cm^{-1}, the peak of MGITC.

To support the experimental findings, theoretical correction calculations were conducted using COMSOL Multiplex (wave optics module). The refractive index of air was set to 1.0, and the gold data were taken from a report published by Johnson and Christy.[42] The results indicate that gold deposited on the grain structure formed after 7 h of heat treatment was more uniform and denser than when the grain structure was formed using a shorter heat-treatment time. This resulted in a more uniform and stronger electromagnetic enhancement at the hotspots on the gold surface (Fig. 3a and b) and indicates that the theoretical and experimental results are in agreement.

To select a suitable Raman laser that can amplify the signal of the established SERS-active substrates, we conducted experiments to calculate the electromagnetic enhancement distribution and compare the SERS signals. This allowed us to determine the laser wavelength that enhanced the SERS efficiency of the substrates. The results of the simulation calculations indicate that the use of lasers with wavelengths of 532, 633, and 785 nm results in electric field (EF) values of 382 960.13, 1 278 292.44, and 362 405.65, respectively. The highest EF was obtained at 633 nm. To experimentally validate the aforementioned findings, the SERS-active substrates were immersed in MGITC at a concentration of 1 μM for 12 h. The SERS signals of the substrate were evaluated as functions of the Raman laser wavelength. The measured SERS spectra represented the average of 20 SERS datasets collected at random locations. As revealed by the simulation results, the SERS intensity of the 633 nm laser was ≈10-fold higher than that of the other laser wavelengths used in the experiment (Fig. 4).

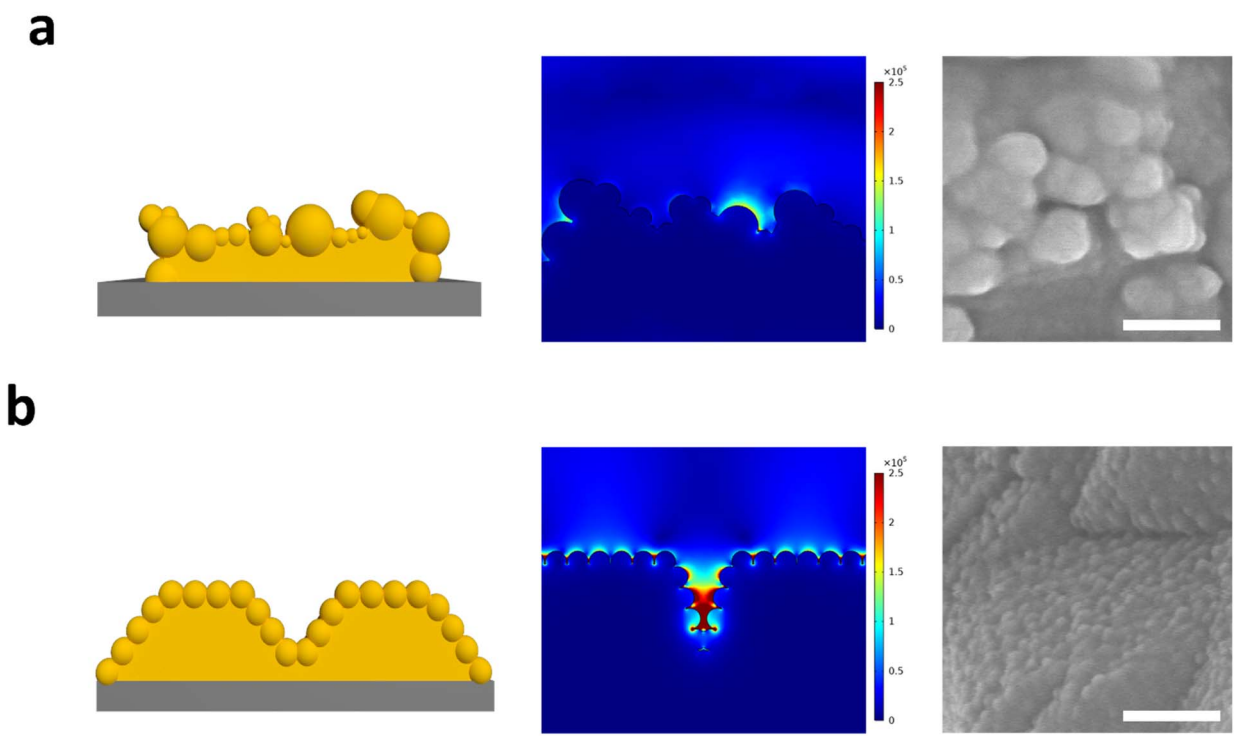

Fig. 3 FEM-simulated electric field distribution schemes and SEM images of substrates with gold deposited on Ni foam after heat treatment for (a) 0.5 h and (b) 7 h. The scale bar represents 100 nm.

 © 2025 The Author(s). Published by the Royal Society of Chemistry

Open Access Article. Published on 13 March 2025. Downloaded on 1/10/2026 1:36:28 PM.
This article is licensed under a Creative Commons Attribution-NonCommercial 3.0 Unported Licence.

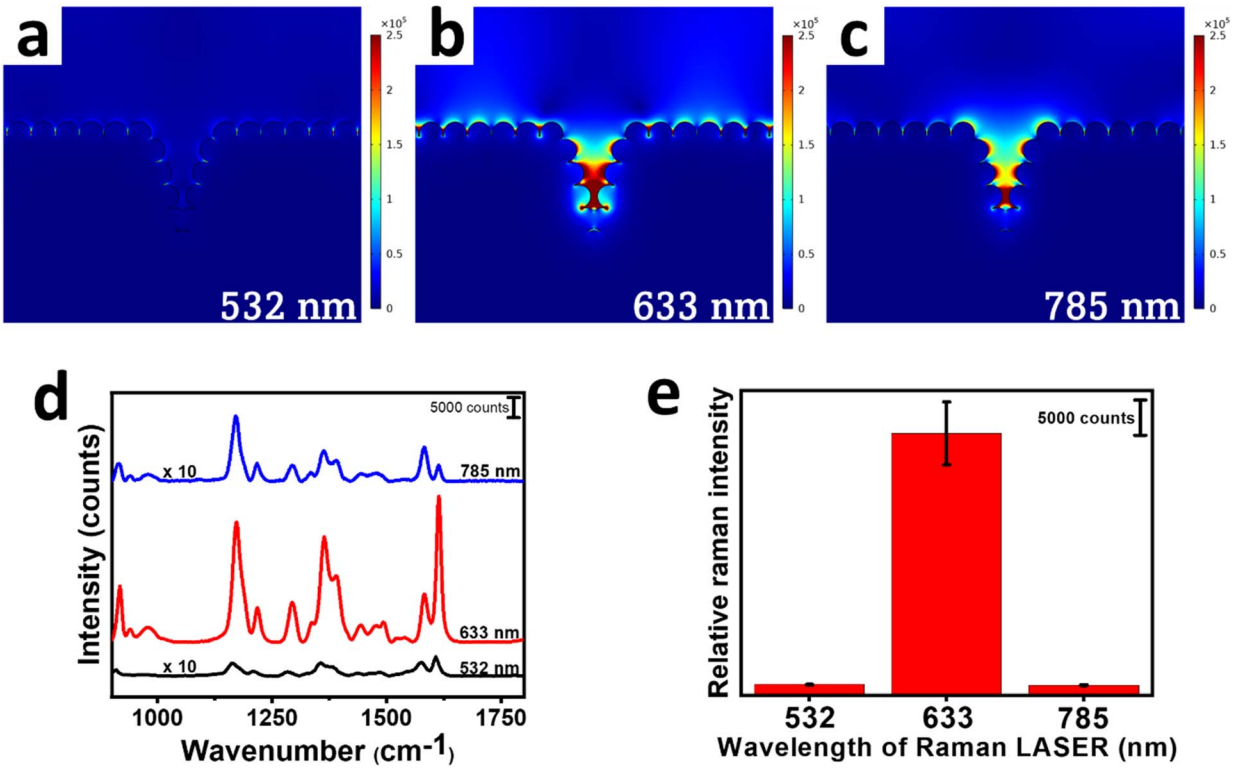

Fig. 4 FEM-simulated electric field distribution of the SERS-active substrates at (a) 532, (b) 633, and (c) 785 nm incident light. (d) Average SERS spectra of SERS-active substrates measured at 532, 633, and 785 nm incident light and (e) comparison of SERS intensity at 1615 cm^{-1}.

In this experiment, we fabricated SERS-active substrates by depositing gold after heat treatment at 800 °C for 7 h and experimentally and theoretically investigated their performance. SERS-active substrates with grain structures formed by annealing can further enhance the SERS signal by providing more hotspots within the same focal volume. To demonstrate this, we compared the SERS signals of pure Ni foam, Ni foam with only gold deposited, and SERS-active substrates. Pure Ni foam was immersed in MGITC at a concentration of 10^{-2} M and Ni foam with only gold deposited, and SERS-active substrates were immersed in MGITC at a concentration of 10^{-7} M for 12 h and rinsed to quantify the SERS signal. As illustrated in Fig. 5a, the substrate with the grain structure formed by heat treatment exhibited a more enhanced SERS signal than the substrate without heat treatment. In comparison to pure Ni foam, the SERS-active substrates exhibited an EF value of 2.65×10^6, which is comparable to that obtained through simulation calculations. Details for their determination were described in ESI.† Fig. 5b and d illustrate the Raman spectra and intensity distributions of MGITC at 20 randomly selected locations on the gold-coated Ni foam with and without the formation of grain structures through heat treatment. This comparison allowed for the assessment of signal uniformity and intensity. Fig. 5c and e present the relative standard deviations (RSDs) of the Raman peak intensity of MGITC at 1615 cm^{-1}. The average Raman signals and RSDs of MGITC at 1615 cm^{-1} were 139 410.13 (29%) and 34 232.47 (12%) when measured with and without heat treatment, respectively. The formation of protruding grain structures *via* heat treatment provided a larger surface area. Furthermore, the deposition of gold on the surfaces of the heat-treated structures was more uniform and exhibited a lower surface energy, which also contributed to the high reproducibility of the signal. SERS mapping data for five different substrates are shown in Fig. S2.† These SERS mapping data clearly demonstrate the reproducibility and signal uniformity of the SERS substrates fabricated in this study. In addition, the surface structures formed by high-temperature annealing are more stable than conventional chemical etching or template-based methods, which enhances the reusability of the substrate. To evaluate the reusability of our SERS substrate, we performed a recyclability test (Fig. S3†). First, SERS signals were measured using MGITC molecules, and then the substrate underwent a plasma cleaning treatment. After the cleaning process, we observed that the SERS signals were effectively eliminated, indicating the successful removal of MGITC molecules from the substrate surface. When the cleaned substrate was re-exposed to MGITC in the second cycle, it exhibited SERS intensities similar to those observed in the first cycle. This consistent signal recovery pattern was maintained through the third cycle, demonstrating the robust reusability of the SERS substrate through multiple cleaning and detection cycles. This approach to SERS substrate fabrication represents a step forward in the practical implementation of SERS substrates by achieving high sensitivity without the need for complex equipment or specialized techniques.

A competitive assay was conducted using a SERS-active substrate to detect troponin I, a cardiac biomarker that can be

Open Access Article. Published on 13 March 2025. Downloaded on 1/10/2026 1:36:28 PM.
This article is licensed under a Creative Commons Attribution-NonCommercial 3.0 Unported Licence.

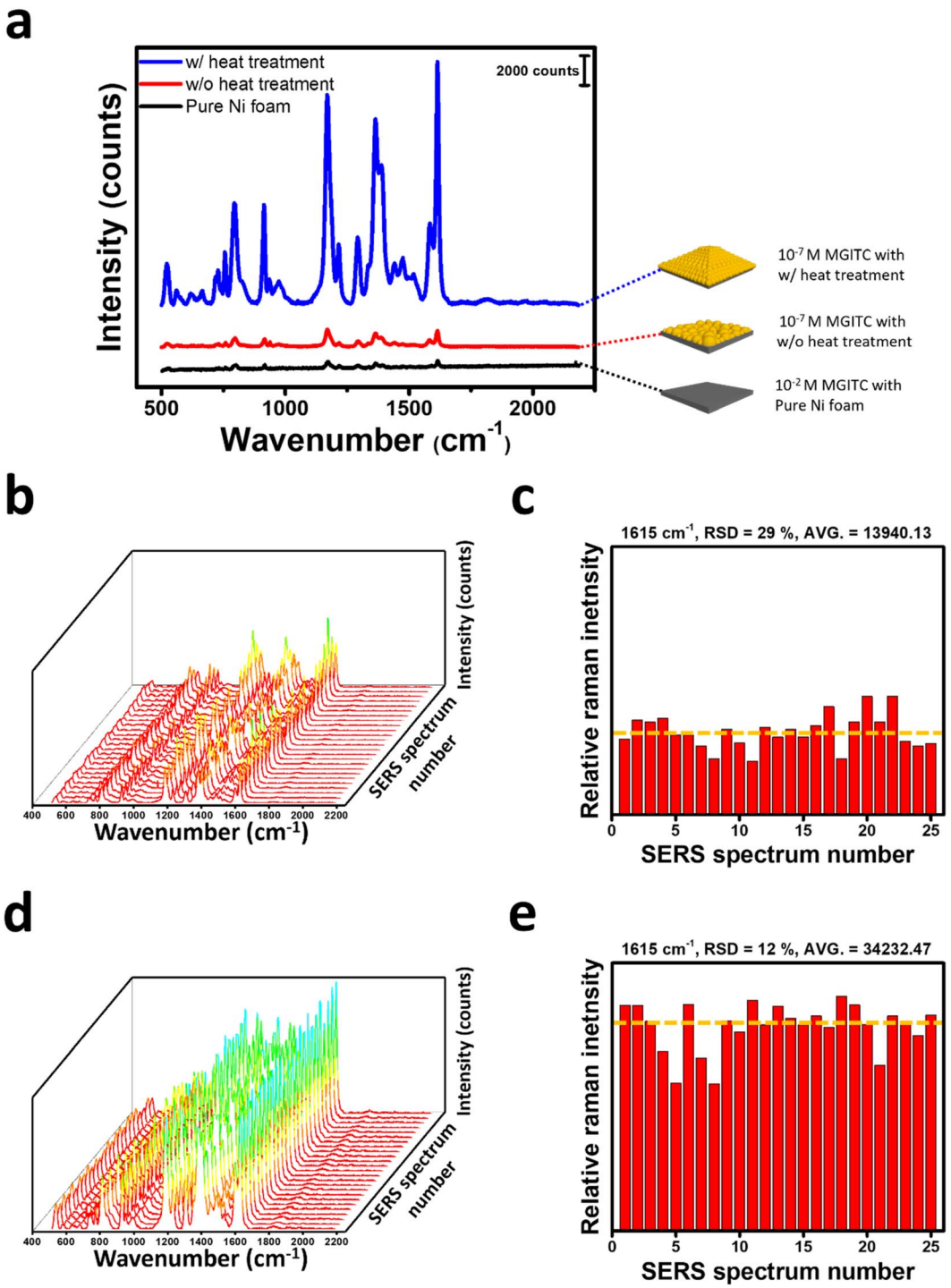

Fig. 5 (a) Comparison of SERS signals for pure Ni foam (with 10^{-2} M of MGITC) and SERS-active substrates with and without heat treatment (with 10^{-7} M of MGITC). SERS spectra of MGITC were measured for 25 spots chosen randomly from substrates (b) without heat treatment and (d) with heat treatment. Raman intensity distributions of the peaks at 1615 cm^{-1} for (c) without heat treatment and (e) with heat treatment substrates.

used to predict the prognosis of heart failure. Competitive assays have the advantages of high specificity and selectivity owing to the use of monoclonal antibodies that react with only one epitope on the target molecule. To confirm the antigen–antibody binding affinity prior to the competition assay, the anti-cTnI antibody was conjugated to MGITC-labeled 50 nm AuNPs, and the capture antigen was immobilized on the SERS-active substrates to enable the antigen–antibody reaction. As illustrated in Fig. 6a, the antibody-conjugated AuNPs bound to the antigen on the SERS-active substrate. To verify the reproducibility of the assay, the aforementioned experiment was repeated five times; the intensities of the measured SERS spectra at 1615 cm^{-1} are compared in Fig. 6b. The RSDs were calculated to be 4.6%, indicating that the antigen–antibody

 © 2025 The Author(s). Published by the Royal Society of Chemistry

Open Access Article. Published on 13 March 2025. Downloaded on 1/10/2026 1:36:28 PM.
This article is licensed under a Creative Commons Attribution-NonCommercial 3.0 Unported Licence.

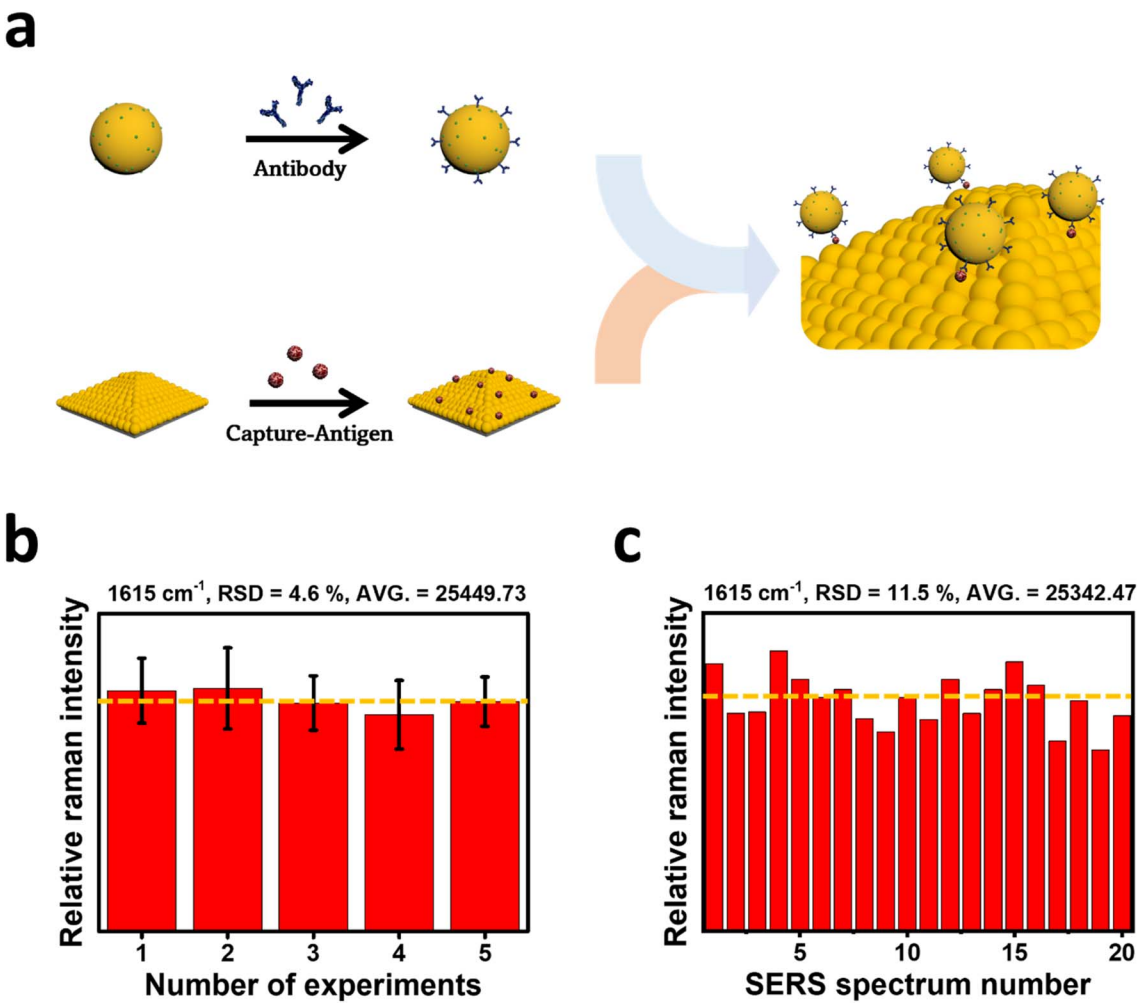

Fig. 6 (a) Scheme of the antigen–antibody reaction after modifying the antibody on the particles and arranging the capture antigen on SERS-active substrates. (b and c) Raman intensity distributions of the 1615 cm^{-1} peaks (b) repeated five times to confirm the reproducibility of the experiment and (c) in 20 SERS signals obtained from one substrate to confirm uniformity.

modification on the AuNPs and SERS active substrate was uniform and specific, resulting in reproducible and accurate results. Furthermore, when 20 random spots were measured, the RSD of the Raman peak intensity of MGITC at 1615 cm^{-1} was 11.5%, thereby confirming that the antigen–antibody reaction occurred uniformly (Fig. 6c). To verify whether the signals were due to non-specific reactions or antigen–antibody interactions, we have conducted comprehensive specificity validation experiments. (Fig. S4†) In our control experiments, when antibody-conjugated gold nanoparticles were introduced to SERS substrates without immobilized recombinant proteins, SERS signals were weak. This demonstrates that our optimized blocking conditions effectively suppress non-specific binding between the substrate and gold nanoparticles. Therefore, we can confirm that the observed signals result from specific antigen–antibody interactions between the immobilized recombinant proteins and antibodies on the gold nanoparticles.

In competition assays, the analyte to be detected is pre-mixed with AuNPs to determine the change in the SERS signal with analyte concentration before the antibody-conjugated AuNPs and the SERS active substrate react with the capture-antigen arranged on it. Fig. 7a illustrates the basic principle of competition assays. If the concentration of the target antigen is low at the time of pre-mixing, as illustrated in Fig. 7a, the antibody conjugated to the AuNPs will possess unoccupied sites that will bind to the capture antigen on the substrate, resulting in a robust SERS signal. Conversely, if the concentration of the target antigen is high at the time of pre-mixing, as in case ii, the probability of the antibody conjugated to the AuNPs binding and reacting with the captured antigen of the SERS-active substrate is low, resulting in a decrease in the SERS signal. The SERS mapping images obtained at 1615 cm^{-1} indicate that the higher the concentration of the target antigen, the more likely the antibody conjugated to the AuNPs completed the reaction and did not react with the captured antigen of the SERS-active substrate, resulting in a weak SERS signal. In this study, recombinant human cTnI was used as the target antigen. Fig. 7b shows that the SERS signal diminishes as the concentration of cTnI increases in the competition analysis. Fig. 7c

Open Access Article. Published on 13 March 2025. Downloaded on 1/10/2026 1:36:28 PM.
This article is licensed under a Creative Commons Attribution-NonCommercial 3.0 Unported Licence.

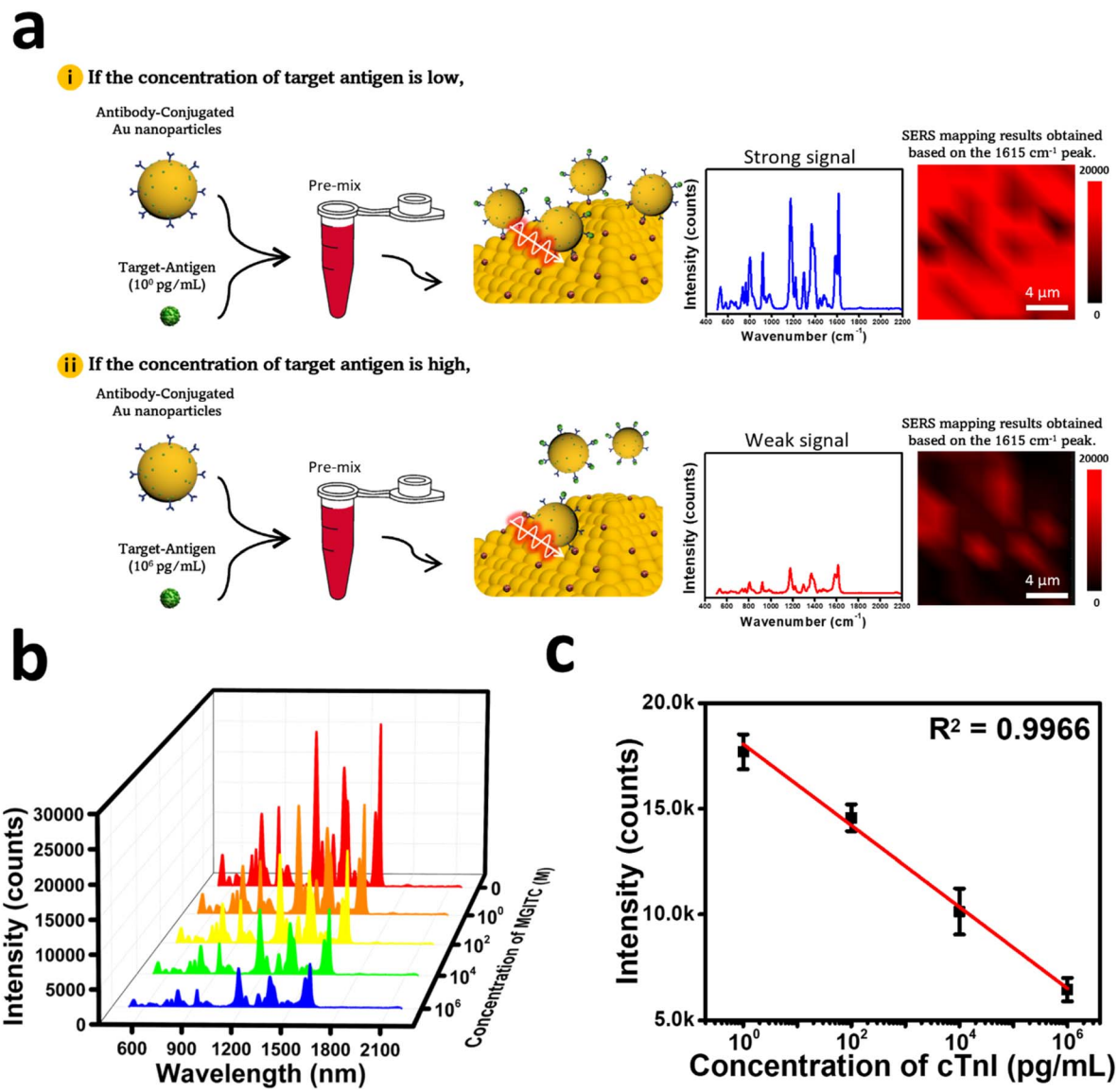

Fig. 7 (a) Schematic of SERS-based competition assay for the detection of cTnI. When pre-mixing, (i) and (ii) represent low and high concentrations of the target antigen, respectively. (b) SERS spectra for increasing concentration of cTnI and (c) corresponding calibration curves of SERS signal intensity at 1615 cm^{-1} for MGITC.

depicts a linear correlation between the respective concentrations and SERS intensity at 1615 cm^{-1}; the R^2 value is 0.9966, which is satisfactory. In conclusion, the competitive assay demonstrated a detection range for cTnI of 10^0–10^6 pg mL^{-1}, with a LOD of 5.8 pg mL^{-1}. These findings confirmed the effectiveness of SERS-active substrates for cTnI biomarker detection.

Conclusions

SERS-active substrates were fabricated using a Ni foam to detect cTnI. The protruding structure was fabricated by heat treatment, and then gold was sputtered to form multiple hotspots on the Ni foam surface. This structure enhanced the SERS signal by providing a large number of hotspots within the same laser focal volume. This was verified by a finite element method (FEM) simulation of the electric-field distribution of the SERS-active substrate in accordance with the incident light and agreed with the experimental results. This study demonstrates that a competition assay employing a SERS-active substrate can be used to detect cTnI in the range of 10^0–10^6 pg mL^{-1}, with a LOD of 5.8 pg mL^{-1}. In conclusion, the SERS-active substrate based on the Ni foam has the potential to be highly sensitive and specific for biomarker detection.

Experimental section

Materials and reagents

Poly(ethylene glycol) 2-mercaptoethyl ether acetic acid (HS-PEG-COOH, molecular weight ≈ 3500), *N*-(3-dimethylaminopropyl)-

 © 2025 The Author(s). Published by the Royal Society of Chemistry

Open Access Article. Published on 13 March 2025. Downloaded on 1/10/2026 1:36:28 PM.
This article is licensed under a Creative Commons Attribution-NonCommercial 3.0 Unported Licence.

N′-ethylcarbodiimide hydrochloride (EDC), 2-(*N*-morpholino) ethanesulfonic acid hydrate (MES), bovine serum albumin (BSA), Triton X-100, and Tween 20 were purchased from Sigma-Aldrich. Malachite green isothiocyanate (MGITC), *N*-hydroxysulfosuccinimide (sulfo-NHS), and 3,3′- (sulfosuccinimidyl propionate) (DTSSP) were purchased from Thermo Fisher Scientific. Phosphate buffered saline (PBS) packs containing 0.1 M sodium phosphate and 0.15 M NaCl buffer at pH 7.2 when dissolved in 500 mL of deionized water were also purchased from Thermo Scientific. Gold-coated magnetic nanoparticles (50 nm, citrate stabilized) were purchased from Nano-ImmunoTechnology. Ni foam (porosity ≈ 98%, Ni ≈ 99.9%, length ≈ 250 mm, thickness ≈ 1.5 mm, pore size ≈ 0.2–0.5 mm, and density ≈ 380 g m^2 ± 20) was obtained from China (Taiyuan Liyuan Lithium Technology Co. Ltd). The anti-cTnI antibody [EPR20307] and recombinant human cTnI protein were purchased from Abcam (Cambridge, UK).

Instruments

Ultraviolet-visible-near-infrared absorption spectra were obtained using a JASCO V-770 spectrophotometer. Field-emission scanning electron microscopy (FE-SEM) images were obtained using a Hitachi S-4300 FE-SEM instrument (SEMIONE, Hanyang University ERICA) at an accelerating voltage of 15 kV. Thermal treatment was performed using thermal chemical vapor deposition (TCVD; Scen Tech, customized instrument) in Ar. An automatic sputter coater with a film thickness monitor (Agar Scientific) was used to form hotspots for 600 s at 20 mA. Raman spectra and mapping images were acquired using confocal micro-Raman spectroscopy with a dark-field microscope (WEVE, HEDA). The following excitation sources were used: a 532 nm single longitudinal mode diode-pumped solid-state laser (DPSS) laser (50 mW; CNI); a 633 nm He–Ne gas laser (17 mW, Newport); and a 785 nm single longitudinal mode DPSS laser (130 mW); (Integrated Optics). Raman scattering signals were collected using a charge-coupled device camera with a high-resolution grating (1200 grooves mm^{-1}) and measured by focusing a laser spot using a 100 × (NA 0.9) objective lens with a diffraction limit of ≈200 nm. The SERS mapping data was measured as 10 × 10 points along the *x*–*y* axis, with a spacing of 2 μM between points. Spectra were obtained with exposure times of 1 s and 3 s for verifying the performance of the SERS-active substrate and for the competition immunoassay, respectively, both with a laser power of 0.4 mW after applying a 10% neutral density filter. For the back-ground subtraction, the mean difference equation was calculated using a window size of 13.

Fabrication of SERS-active substrates based on Ni foam

The SERS-active substrates on the Ni foam were fabricated by thermally treating the Ni foam, followed by Au deposition. Ni foam was first acid-treated to ensure purity. It was sonicated with 3 M hydrochloric acid (HCl) for 20 min with continuous stirring, followed by three rinses with water for 5 min, and rinsing twice with acetone for 10 min before being dried in an oven. The surface of the Ni foam was then modified by thermal treatment to create a bumpy structure, which was placed on an alumina boat inside the CVD system and vacuumed to a low pressure (≈10^{-3} torr). The temperature was raised to 800 °C by flowing 1000 sccm of Ar gas at a slow heating rate of 5 °C min^{-1} and held for 7 h. Finally, heating was terminated, and the sample was cooled to room temperature (25 °C). Subsequently, Au was deposited to form hotspots on the protruding Ni foam using an automatic sputter coater with a film thickness monitor for 600 s at 20 mA.

Preparation of antibody-conjugated SERS nanotags

Gold nanoparticles (AuNPs) with a diameter of 50 nm (Merck, Temecula, USA) were prepared as a solution. Then, 1 mL of AuNP solution was mixed with 1 μL of 3% Tween 20 and reacted for 10 min under vortexing to reduce AuNP aggregation. MGITC (3 μL, 100 μM) was added to the AuNP solution and gently mixed for 40 min. Afterwards, the solution was treated with 100 μM SH-PEG-COOH for 2 h to modify the AuNP surface with carboxyl groups. After the reaction, the solution was centrifuged (6000 rpm, 10 min) twice and redispersed in MES buffer. To convert the carboxyl groups to amine groups, 10 μL of 1 mM EDC/NHS solution was added, and the solution was vortexed for 30 min. Centrifugation (6000 rpm, 10 min) was performed to remove the unreacted EDC/NHS solution, which was redispersed in 10× PBS buffer. Next, 20 μL of cTnI antibodies (100 μg mL^{-1}) were reacted with the solution overnight. The antibody-conjugated AuNPs were centrifuged (6000 rpm, 10 min) and redispersed in 1 mL of 10× PBS buffer. Finally, 50 μL of blocking buffer (1.575% BSA + 1.575% Triton X-100 in 10× PBS buffer) was added to prohibit non-specific binding on the SERS nanotags. The SERS nanotags were centrifuged (6000 rpm, 10 min) and redispersed in 500 μL of 10× PBS buffer. For the competition assay, antibody-conjugated SERS nanotags were premixed with a specific concentration of the target antigen for 1 h. Unreacted target antigens were removed by centrifugation (6000 rpm, 10 min), and the sediments were dispersed in 10× PBS buffer.

Surface modification of SERS-active substrates on Ni foam

The SERS-active substrates were treated with 5 mM DTSSP as a linker for 1 h. Then, the substrates were washed thrice with 1 mL of distilled water. The captured antigens for cTnI were immobilized on SERS-active substrates using linkers. Capture antigens (10 μg mL^{-1}) were added and incubated overnight. The SERS-active substrates were then washed three times with 1 mL of 10 × PBS buffer. A blocking buffer solution (1% BSA + 1% Triton X-100 in 10× PBS buffer) was added and incubated for 1 h to prevent nonspecific binding to the substrates. After washing thrice with 1 mL of 10× PBS buffer, the SERS-active substrates were allowed to react with the pre-mixed SERS nanotags for 1 h. Finally, the substrate was washed thrice with 1 mL of 10 × PBS buffer.

Open Access Article. Published on 13 March 2025. Downloaded on 1/10/2026 1:36:28 PM.
This article is licensed under a Creative Commons Attribution-NonCommercial 3.0 Unported Licence.

Data availability

COMSOL Multiphysics® v. 5.6, to perform the modelling can be found at https://www.comsol.com/support/knowledgebase/1223. The authors confirm that the data supporting the findings of this study are available within the article. The authors will supply the relevant data in response to reasonable requests.

Author contributions

S. H. Yoo and J. J. Park contributed equally to the investigation, data analysis, methodology, and writing of the original manuscript. D. H. Nam and S. M. Kim contributed to formal analysis. M. Lee contributed to manuscript editing. S. H. Lee supervised and contributed to conceptualization, methodology, manuscript review, and editing. All authors read and approved the manuscript.

Conflicts of interest

There are no conflicts to declare.

Acknowledgements

This research was supported by the National Research Foundation of Korea grants (RS-2024-00339674 and 2021M3H4A4080400) and the GRRC program of Gyeonggi Province (GRRC Hanyang 2020-B03). D. J. was supported by grants from the National Research Foundation of Korea (RS-2021-NR058338 and RS-2024-00440285) funded by the Korean Government (MSIP).

References

1 Z. Cheng, R. Wang, Y. Xing, L. Zhao, J. Choo and F. Yu, *Analyst*, 2019, **144**, 6533–6540.
2 C. Hu, L. Ma, M. Guan, F. Mi, F. Peng, C. Guo, S. Sun, X. Wang, T. Liu and J. Li, *Anal. Methods*, 2020, **12**, 5442–5449.
3 R. S. Alves, F. A. Sigoli and I. O. Mazali, *Nanotechnology*, 2020, **31**, 505505.
4 Z. Yuan, L. Wang, J. Chen, W. Su, A. Li, G. Su, P. Liu and X. Zhou, *Analyst*, 2021, **146**, 5474–5495.
5 A. Ahmadi, S. M. Khoshfetrat, Z. Mirzaeizadeh, S. Kabiri, J. Rezaie and K. Omidfar, *Talanta*, 2022, **237**, 122911.
6 N. Wongkaew, M. Simsek, C. Griesche and A. J. Baeumner, *Chem. Rev.*, 2019, **119**, 120–194.
7 J. G. Brussasco, P. H. G. Guedes, A. C. R. Moço, D. D. Moraes, J. M. R. Flauzino, H. S. Silva, A. C. Silva, J. P. Silva, J. M. Madurro and A. G. Brito-Madurro, *J. Mol. Recognit.*, 2023, **36**, e2995.
8 X. Qian, X. Zhou, X. Ran, H. Ni, Z. Li, Q. Qu, J. Li, G. Du and L. Yang, *Biosens. Bioelectron.*, 2019, **130**, 214–224.
9 O. Karaman, N. Özcan, C. Karaman, B. B. Yola, N. Atar and M. L. Yola, *Mater. Today Chem.*, 2022, **23**, 100666.
10 X. Wang, X. Wang, Y. Han, H. Li, Q. Kang, P. Wang and F. Zhou, *ACS Appl. Nano Mater.*, 2019, **2**, 7170–7177.
11 R. Radha, S. K. Shahzadi and M. H. Al-Sayah, *Molecules*, 2021, **26**, 4812.
12 K. W. Lee, K. R. Kim, H. J. Chun, K. Y. Jeong, D. K. Hong, K. N. Lee and H. C. Yoon, *Biosens. Bioelectron.*, 2020, **163**, 112284.
13 Y. Cai, K. Kang, Q. Li, Y. Wang and X. He, *Molecules*, 2018, **23**, 1102.
14 Y. Li, W. Dai, X. Lv and Y. Deng, *Anal. Methods*, 2018, **10**, 1767–1773.
15 S.-W. Kim, I.-H. Cho, J.-N. Park, S.-M. Seo and S.-H. Paek, *Sensors*, 2016, **16**, 669.
16 K. Lang, A. Borner and H. R. Figulla, *J. Intern. Med.*, 2000, **247**, 119–123.
17 M. A. Rezaee, M. J. Rasaee and J. Mohammadnejad, *J. Immunoassay Immunochem.*, 2017, **38**, 72–81.
18 C. Heeschen, B. U. Goldmann, L. Langenbrink, G. Matschuck and C. W. Hamm, *Clin. Chem.*, 1999, **45**, 1789–1796.
19 S. Y. Song, Y. D. Han, K. Kim, S. S. Yang and H. C. Yoon, *Biosens. Bioelectron.*, 2011, **26**, 3818–3824.
20 L. Miao, L. Zhang, L. Jiao, X. Tan, Q. Wei and H. Li, *Chin. Chem. Lett.*, 2017, **28**, 1878–1880.
21 K. M. Mayer, S. Lee, H. Liao, B. C. Rostro, A. Fuentes, P. T. Scully, C. L. Nehl and J. H. Hafner, *ACS Nano*, 2008, **2**, 687–692.
22 S. Yoo, G. Youn, H. Lee, J. Kwon, Y. Lee and S. Lee, *Bull. Korean Chem. Soc.*, 2023, **2**, 687–692.
23 S. M. Lee, D. H. Nam, D. Lee, S. H. Lim, S. J. Son and S. Lee, *ACS Appl. Nano Mater.*, 2021, **4**, 12905–12912.
24 S. Lee, P. Kumar, Y. Hu, G. J. Cheng and J. Irudayaraj, *Chem. Commun.*, 2015, **51**, 15494–15497.
25 Y. Hu, S. Lee, P. Kumar, Q. Nian, W. Wang, J. Irudayaraj and G. J. Cheng, *Nanoscale*, 2015, **7**, 19885–19893.
26 S. Balamurugan, K. M. Mayer, S. Lee, S. A. Soper, J. H. Hafner and D. A. Spivak, *J. Mol. Recognit.*, 2013, **26**, 402–407.
27 S. Yoo, D. H. Nam, T. I. Singh, G. Leem and S. Lee, *Nano Converg.*, 2022, **9**, 1–9.
28 M. Lu, Y. Joung, C. S. Jeon, S. Kim, D. Yong, H. Jang, S. H. Pyun, T. Kang and J. Choo, *Nano Converg.*, 2022, **9**, 39.
29 H. Kim, H. J. An, J. Park, Y. Lee, M. S. Kim, S. Lee, N. D. Kim, J. Song and I. Choi, *Nano Converg.*, 2022, **9**, 23.
30 S. Kim, S. Yoo, D. H. Nam, H. Kim, J. H. Hafner and S. Lee, *Nano Converg.*, 2024, **11**, 26.
31 B. N. Khlebtsov, D. N. Bratashov, N. A. Byzova, B. B. Dzantiev and N. G. Khlebtsov, *Nano Res.*, 2019, **12**, 413–420.
32 T. Bai, M. Wang, M. Cao, J. Zhang, K. Zhang, P. Zhou, Z. Liu, Y. Liu, Z. Guo and X. Lu, *Anal. Bioanal. Chem.*, 2018, **410**, 2291–2303.
33 D. J. Lee and D. Y. Kim, *Sci. Rep.*, 2021, **11**, 1–9.
34 S. Lee, K. M. Mayer and J. H. Hafner, *Anal. Chem.*, 2009, **81**, 4450–4455.
35 Y. M. Lee, S. E. Kim and J. E. Park, *Nano Converg.*, 2023, **10**, 34.
36 W. Tao, F. Laible, A. Hmima, T. Maurer and M. Fleischer, *Nano Converg.*, 2023, **10**, 15.

 © 2025 The Author(s). Published by the Royal Society of Chemistry

Open Access Article. Published on 13 March 2025. Downloaded on 1/10/2026 1:36:28 PM.
This article is licensed under a Creative Commons Attribution-NonCommercial 3.0 Unported Licence.

37 R. Z. Tan, A. Agarwal, N. Balasubramanian, D. L. Kwong, Y. Jiang, E. Widjaja and M. Garland, *Sens. Actuators, A*, 2007, **139**, 36–41.
38 S. Lee, M. G. Hahm, R. Vajtai, D. P. Hashim, T. Thurakitseree, A. C. Chipara, P. M. Ajayan and J. H. Hafner, *Adv. Mater.*, 2012, **24**, 5261–5266.
39 A. Bozdogan, R. F. El-kased, V. Jungbluth, W. Knoll, J. Dostalek and A. Kasry, *R. Soc. Open Sci.*, 2020, **7**, 200871.
40 M. Grdeń, M. Alsabet and G. Jerkiewicz, *ACS Appl. Mater. Interfaces*, 2012, **4**, 3012–3021.
41 H. Geaney, D. McNulty, J. O'Connell, J. D. Holmes and C. O'Dwyer, *J. Electrochem. Soc.*, 2016, **163**, A1805–A1811.
42 P. B. Johnson and R. W. Christy, *Phys. Rev. B*, 1972, **6**, 4370–4379.